metals

MDPI

Article

Effect of Indium on the Properties of Mg-Zn-Based Alloys

Kamil Kowalski [1], Mikolaj Kozlowski [1,*], Natalia Lukaszkiewicz [1], Mateusz Kobus [1], Jakub Bielecki [1] and Mieczyslaw Jurczyk [2]

[1] Institute of Materials Science and Engineering, Poznan University of Technology, Jana Pawła II 24, 61-138 Poznań, Poland; kamil.kowalski@put.poznan.pl (K.K.); natalia.lukaszkiewicz@student.put.poznan.pl (N.L.); mateusz.kobus@student.put.poznan.pl (M.K.); jakub.bielecki@student.put.poznan.pl (J.B.)

[2] Department of Biomedical Engineering, Institute of Materials and Biomedical Engineering, Faculty of Mechanical Engineering, University of Zielona Gora, Prof. Z. Szafrana 4, 65-516 Zielona Gora, Poland; m.jurczyk@iimb.uz.zgora.pl

* Correspondence: mikolaj.kozlowski@put.poznan.pl

Abstract: In this study, indium was added to the binary Mg-Zn alloy to prepare an ultrafine-grained ternary Mg-Zn-In alloy with enhanced mechanical and corrosion properties. The bulk Mg-Zn-In alloy was synthesized through a combination of mechanical alloying and powder metallurgy techniques. The SPEX 8000 mixer mill was used to carry out the process under an argon atmosphere. The mixed powders were mechanically alloyed for 24 h. The mixture was uniaxially pressed at a compacting pressure of 600 MPa. The green compacts were sintered under a protective argon atmosphere at 300 °C for 1 h. The evolution of the microstructural, mechanical, and corrosion properties of Mg-based alloys was studied. X-ray diffraction and scanning electron microscopy were used to analyze the phase and microstructure. The changes in hardness and corrosion properties were also measured. Compared to binary Mg-Zn alloy samples modified with In, the samples exhibited a higher microhardness, which can be related to structure refinement and phase distribution. Based on the results of electrochemical testing, it was observed that the modified samples exhibited an improved level of corrosion resistance compared to the Mg-Zn binary alloy.

Keywords: magnesium; zinc; indium; mechanical alloying

Citation: Kowalski, K.; Kozlowski, M.; Lukaszkiewicz, N.; Kobus, M.; Bielecki, J.; Jurczyk, M. Effect of Indium on the Properties of Mg-Zn-Based Alloys. *Metals* **2023**, *13*, 1786. https://doi.org/10.3390/met13101786

Academic Editor: Hüseyin Zengin

Received: 27 September 2023
Revised: 19 October 2023
Accepted: 20 October 2023
Published: 22 October 2023

1. Introduction

Magnesium (Mg) [1–3] and its alloys with iron (Fe) [4,5] and zinc (Zn) [6,7] have been extensively studied as potentially biodegradable materials for use in biomedical applications such as endovascular stents, bone pins, and screws. Their mechanical properties, corrosion behavior, and biocompatibility have been enhanced to meet clinical standards. However, Fe alloys corrode slowly in vivo. Magnesium and its alloys corrode too rapidly, and Mg-Zn alloys have unsatisfactory mechanical properties for biomedical applications [8].

Magnesium and its alloys are the preferred materials for implants in bone and blood vessels due to their numerous advantages. Compared to other biomaterials, magnesium has a greater fracture toughness than ceramic and polymer biomaterials. In addition, its elastic modulus and compressive yield strength are more similar to those of natural bone than commonly utilized metallic implants like stainless steel or titanium-based alloys [1,2]. Mg-based biomaterials have been found to have mechanical properties that are comparable to those of human bones. This means that they can help prevent the stress-shielding effect. Magnesium-based biomaterials have gained a high amount of attention in biomedical applications due to their excellent biocompatibility and the fact that magnesium is a naturally occurring element in bone tissue. These properties make Mg-based biomaterials a highly promising option for a wide range of biomedical applications where biocompatibility is crucial. Therefore, the use of Mg-based biomaterials can lead to better clinical outcomes

and improved patient care. It is worth noting that high levels of magnesium in bone tissue have been found to stimulate osteoblastic activity, which promotes the growth of new bone tissue. This could lead to the complete replacement of implants with bone tissue, which is a highly desirable outcome in biomedical applications. Therefore, Mg-based biomaterials are not only able to prevent stress-shielding, but they can also actively promote the growth of new bone tissue, making them an even more attractive option for biomedical applications. Magnesium is known to corrode into soluble, non-toxic products, which makes it a highly desirable material for biomedical applications. Furthermore, the human body is able to tolerate large amounts of magnesium, and any excess magnesium ions are easily excreted in urine. This means that Mg-based biomaterials are not only biocompatible, but also safe for use in the body. Overall, the unique properties of magnesium make it an attractive option for the development of innovative biomaterials that can improve patient outcomes.

Poor corrosion resistance in human body fluids and high rates of hydrogen evolution and alkalization of surrounding tissues are the main limitations of using pure magnesium as a biomaterial [2]. The implant connection can weaken due to these factors, causing decreased mechanical integrity before tissue fully heals. Mg-based materials also have a low hardness and relatively poor tribological properties, further limiting their use in implantology. To overcome these limitations, several methods have been developed to improve the properties of magnesium-based biomaterials. One of the most effective ways to improve the properties of magnesium alloys is the modification of their chemical composition [9–11].

Zinc [12–16], manganese [17], and calcium [18,19] are considered safe and biocompatible options to enhance the characteristics of magnesium alloys. These elements are naturally present in large amounts in the human body and have essential roles in enzyme functions. When added to magnesium, calcium, and zinc can enhance both its mechanical properties and its resistance to corrosion. Zinc, in particular, is highly abundant in the human body and has a strong safety profile for use in biomedical applications. Additionally, Zn can improve the corrosion resistance and mechanical strength of magnesium alloys through solid solution hardening, which reduces the amount of hydrogen released during corrosion. Studies have shown that increasing the mass fraction of zinc in magnesium can effectively reduce the corrosion rate of the alloy. This is a significant finding, as corrosion can lead to implant failure and other complications in biomedical applications. Therefore, by adjusting the mass fraction of zinc in Mg-based biomaterials, researchers can improve their corrosion resistance and enhance their overall performance. This is a promising development in the field of biomaterials, as it can lead to the development of more durable and reliable biomedical implants that can improve patient outcomes [20,21].

Indium is another element that can alter the properties of magnesium-based alloys. It can reduce the grain size of magnesium solid solutions [22], yet can increase the overall corrosion of magnesium alloys [23,24]. Zengin et al. investigated the impact of indium addition on the mechanical properties of AM60 magnesium alloys, both in as-cast and hot-rolled states [23]. The alloys were subjected to different amounts of In, accordingly 0.2%, 0.5%, and 1.0% (wt.%). Before the testing, the alloys went through a series of processes. Firstly, they were cast to form their initial shape. Secondly, they were homogenized for 24 h at a temperature of 350 °C to ensure consistency in their composition. Finally, the alloys underwent hot-rolling with a 40% thickness reduction at 350 °C to enhance their mechanical properties. As a result of the addition of indium to the alloy, the grain size decreased and the solid solution strengthening effect started to increase, resulting in improved mechanical properties including both strength and elongation. The corrosion of binary Mg-In alloys is accompanied by the negative difference effect—a strong hydrogen evolution during galvanostatic polarization. According to Bao et al. [25], adding indium to Mg reduces hydrogen evolution during corrosion, as it reduces the negative difference effect of Mg alloys with increasing indium metal contents and leads to decreased anodic current densities.

Mechanical alloying (MA) allows us to synthesize various non-equilibrium phases such as amorphous alloys or supersaturated solid solutions during the solid-state process. In crys-

talline materials, the severe plastic deformation process of MA can lead to particle refinement down to the nanometer scale. Starting materials containing high-purity powders are subjected to repeated cold-welding and crushing, which lead to a reduction in the crystallite size of the materials and affects the final microstructure of the materials [12,26–28].

MA combined with powder metallurgy is an effective way to alter the properties of magnesium-based materials [12,28–30]. Recently, Salleh et al. [31] produced binary Mg-Zn alloys via the mechanical alloying and powder metallurgy route. As the milling time increased up to 10 h, the refinement of the particle size led to an improvement in the density and microhardness. However, further milling time caused excessive heat generation and a decreased densification effect.

Yang et al. [32] used MA to prepare Mg-Zn solid solution powders combined with powder bed fusion laser sintering. The powder that had been milled for 30 h showed enhanced corrosion properties and a reduced corrosion rate with good biocompatibility. Hu et al. [33] used the planetary ball mill for 5 h to produce Mg-Zn binary alloys with different contents of zinc. Their study suggests that, for biomedical applications, Mg-20 wt.% Zn is the most suitable alloy. With the compression strength reaching up to 320 MPa and the maximum bending strength (190 MPa) combined with improved corrosion properties, this alloy could be a possible candidate for implant production.

Due to the low melting temperature, the mechanical alloying of magnesium and its alloys can be demanding. Youseff et al. [34] suggest that the agglomeration of powder to the vial walls results in inhomogeneous milling because the plastic deformation occurs only in the top layer of milled powders. Various methods can be used to prevent or reduce the agglomeration of powders in the vial. One of the most effective ways is adding a process control agent (PCA). However, the presence of additional substances such as heptane, methanol, or stearic acid can affect the final properties of milled powders. Another way to reduce the agglomeration of powders is the modification of the mill via the addition of rotational and sliding movement [35]. One of the methods that can be employed to avoid excessive agglomeration and dissipate heat from the vial is milling in a discontinuous process. This technique involves the periodical interruption of the milling process, allowing the vial to cool down and preventing the formation of clumps in the material being milled. Using discontinuous milling, we can improve the quality of the milled product, while also minimizing the risk of excessive heating and eliminating the risk of contamination by the PCA [29,30,34,36,37].

In the present work, the effect of indium addition on the properties of the Mg-20Zn alloy was studied. The bulk Mg-Zn-In alloy was synthesized using a combination of mechanical alloying and a powder metallurgy technique. These studies aimed to determine the optimal MA time to obtain a Mg-Zn-In ternary alloy with optimized properties for future biomedical applications.

2. Materials and Methods

Both the Mg-20 wt.% Zn and Mg-20 wt.%Zn-1 wt.% In alloys were prepared using the MA and powder metallurgy technique. Pure elemental powders of magnesium (99.8% purity, with particle size of 325 mesh; Alfa-Aesar, Haverhill, MA, USA), zinc (99.0% purity, Sigma-Aldrich, St. Louis, MO, USA; maximum particle size of 110 mesh), and indium (99.9% purity, with particle size of 100 mesh; Alfa-Aesar, Haverhill, MA, USA) were used as initial materials. The elemental powders were weighed, mixed, and poured into a round-bottom stainless vial with grinding balls made of Cr-tempered steel in a glove box (Labmaster 130, MBraun, München, Germany) filled with an automatically controlled argon atmosphere (O_2 2 ppm and $H_2O \leq 1$ ppm) to obtain the nominal composition Mg-20 wt% Zn-1 wt%. Table 1 summarizes the parameters used to manufacture the samples.

Mechanical alloying was performed for 12, 24, 36, and 48 h at ambient temperature without a process control agent using an SPEX 8000M Mixer Mill (Metuchen, NJ, USA) with a Ball to Powder Ratio (BPR) of 20:1 in continuous mode. To create the bulk alloys, powder metallurgy was utilized. Initially, the powders underwent uniaxial pressing with a

compacting pressure of 600 MPa. The resulting samples had dimensions of d = 8 mm in diameter and h = 4 mm in height. Lastly, the green compacts were sintered under a vacuum atmosphere at 300 °C for 1 h to form bulk samples.

Table 1. Preparation conditions of the studied materials.

Sample	Mg-20Zn	Mg-20Zn-1In			
MA time [h]	48	12	24	36	48
BPR	20:1	20:1			
Compacting pressure [MPa]	600	600			
Sintering conditions	300 °C/1 h/vacuum	300 °C/1 h/vacuum			

Before testing, the bulk alloys Mg-20Zn and Mg-20Zn-1In were ground with 1200 grit SiC paper in water, then were polished in 0.05 µm alumina suspension and ultrasonically rinsed with acetone.

The as-milled and sintered samples were characterized for morphology and chemical composition using scanning electron microscopy (SEM, Mira 3, Tescan, Brno, Czech Republic) and energy-dispersive X-ray spectroscopy. The scanning electron microscope was equipped with an EDS-UltimMax energy dispersive spectrometer (Oxford Instruments, High Wycombe, UK) and dedicated Aztec Energy Live Standard software (ver. 6.0, Oxford Instruments, High Wycombe, UK). During the EDS study, 15 kV of energy was used. The phase composition of the specimens was analyzed using an EMPYREAN PANalytical X-ray diffractometer (Malvern Panalytical Ltd., Malvern, UK) operating in the range of $2\theta = 30–80°$ using Cu Kα radiation (λ = 1.54056 Å) with the following parameters: voltage, 45 kV; anode current, 40 mA; time per step, 60.325 s/step; and step size, 0.0334°.

The densities of the sintered samples were determined using the Archimedes method. The porosity of the porous materials was calculated using the formula $P = (1 - \rho/\rho_{th}) \times 100\%$, where ρ and ρth are the density of the porous material and its theoretical density (calculated via the rule of mixtures), respectively.

The microhardness of the samples was measured using the Vickers method, based on the PN-EN ISO 6507-1:2018-05 standard [38], using the INNOVATEST Nexus 4302 (INNOVATEST Europe BV, Maastricht, The Netherlands). First, the samples were polished, and then 5 indents per sample were made, under a load of 300 g with an operating time of 10 s, to obtain an average value for the microhardness.

To determine the corrosion resistance of various samples in the Ringer solution (simulated body fluid (SBF) containing aggressive chloride ions, with the following composition: NaCl: 9 g/L, KCl: 0.42 g/L, $CaCl_2$: 0.48 g/L, $NaHCO_3$: 0.2 g/L), the potentiodynamic mode was employed with a scan rate of 0.5 mV/s at a temperature of 37 ± 1 °C, controlled by a thermostat. The Solartron 1285 potentiostat (Solartron Analytical, Farnborough, UK) was utilized for the experiment. The corrosion test was carried out using the EG&G K0047 corrosion cell. A three-electrode setup was used for these studies. For the counter electrode, two graphite rods were used, while a saturated calomel electrode (SCE) was utilized as the reference electrode. The surface area that was exposed to the electrolyte was 0.5 cm^2. To estimate the corrosion potentials (E_c) and corrosion current densities (I_c), the Tafel extrapolations of the polarization curves were analyzed through the use of CorrView software (version 3.5j, Scribner LLC, Southern Pines, NC, USA).

3. Results

The effect of mechanical alloying on the structure and powder morphology was studied. Figures 1 and 2 depict the XRD patterns and SEM images of initial powders. All of the powders used have a microcrystalline structure with sharp peaks. Magnesium and zinc powder particles have irregular shapes, whereas indium powder particles are close to spherical (Figure 2). The particle size distribution for Mg and In is similar, whereas Zn powder consists of large particles.

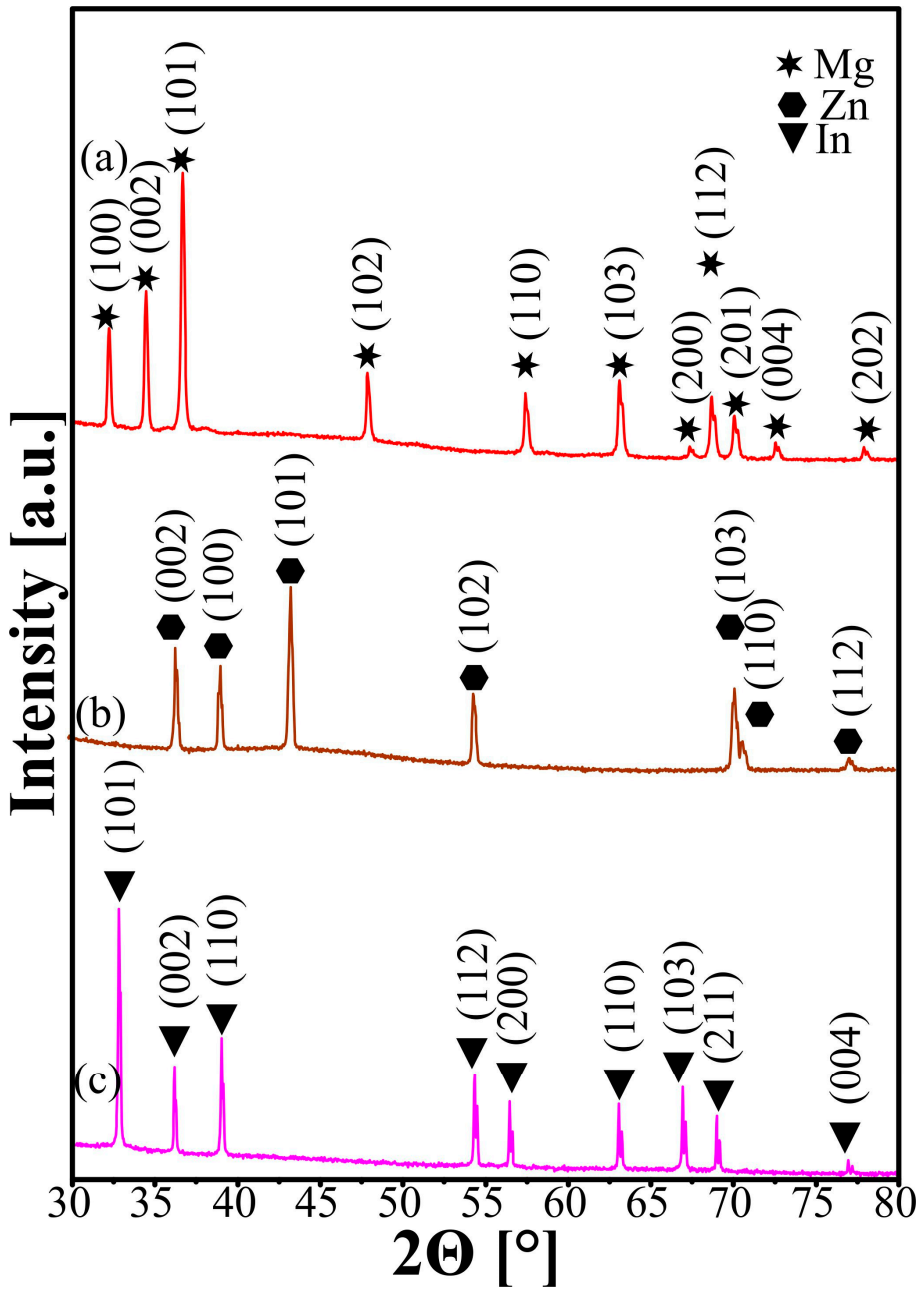

Figure 1. XRD patterns of the initial powders: magnesium (**a**), zinc (**b**), and indium (**c**).

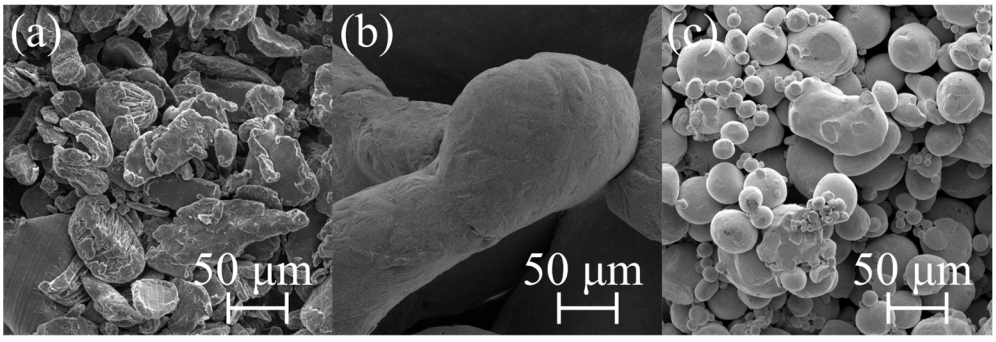

Figure 2. SEM images of the initial powders: magnesium (**a**), zinc (**b**), and indium (**c**).

The effect of MA on the shape and distribution of powders is presented in Figures 3 and 4. Initially, the peak of Zn is visible in the XRD spectrum but, after 6 h of MA, Zn dissolves completely in the Mg matrix. Up to 48 h of milling on the patterns, only peaks from the α-Mg phase are visible. The peak positions for the major-phase magnesium shifted to lower angles, consistent with the dissolved Zn and In in the matrix. The alloy's structure consisted of a small-grained hcp α-Mg phase, with an average crystallite size of 30 nm, determined via the Williamson–Hall method.

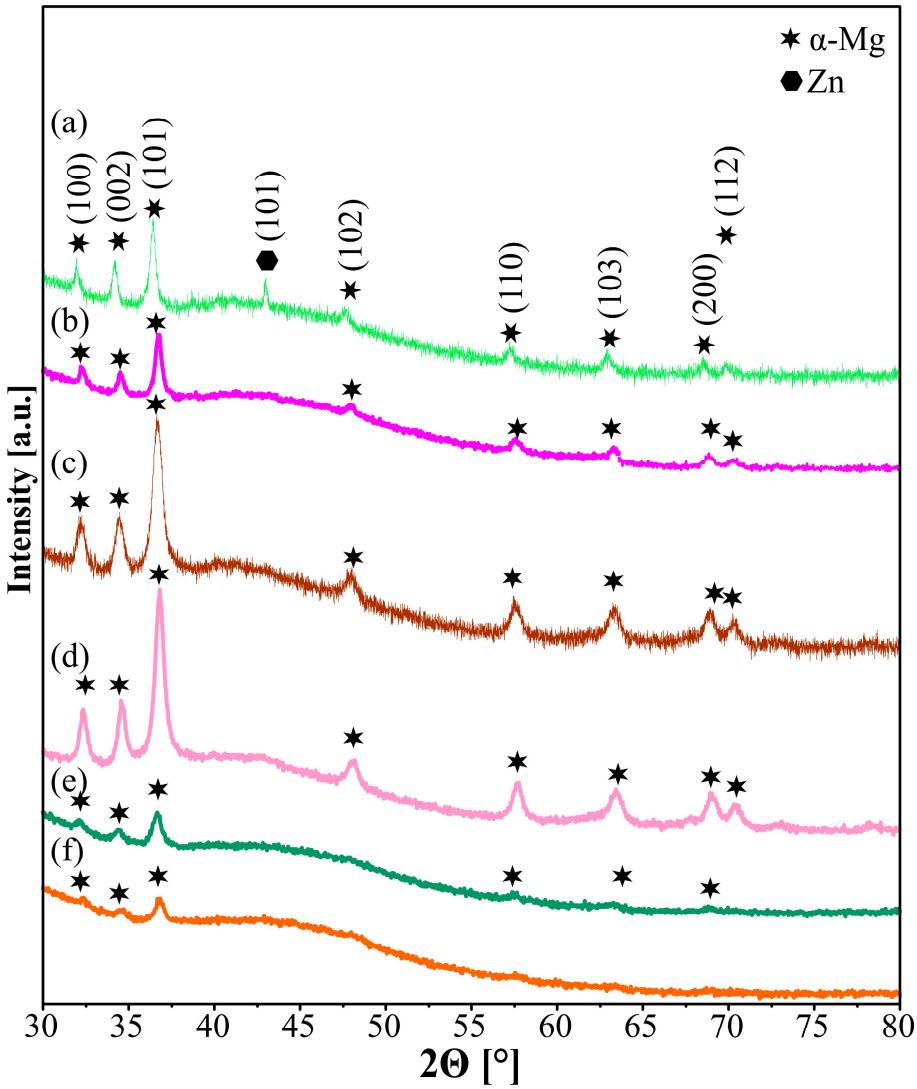

Figure 3. XRD patterns of the as-milled powders after mechanical alloying: 3 h (**a**), 6 h (**b**), 12 h (**c**), 24 h (**d**), 36 h (**e**), and 48 h (**f**).

During the process of mechanical alloying, it can be observed that the powder particles tend to form agglomerates of varying sizes, ranging from the nanometric to micrometric scales. Based on the SEM BSE images presented in Figure 4, it is evident that the magnesium matrix displays a relatively uniform distribution of both Zn and In the following 12 h of MA. This observation suggests that the mechanical alloying process has resulted in the successful dispersion of Zn and In within the magnesium matrix. As the milling time increases, the agglomerates and aggregates reduce in size considerably. This phenomenon can be attributed to the intense pressure and shear forces generated during the milling process, which break down the larger particles into smaller ones, resulting in a more uniform and fine powder. There are no visible signs in the XRD patterns or the images of the presence of other phases.

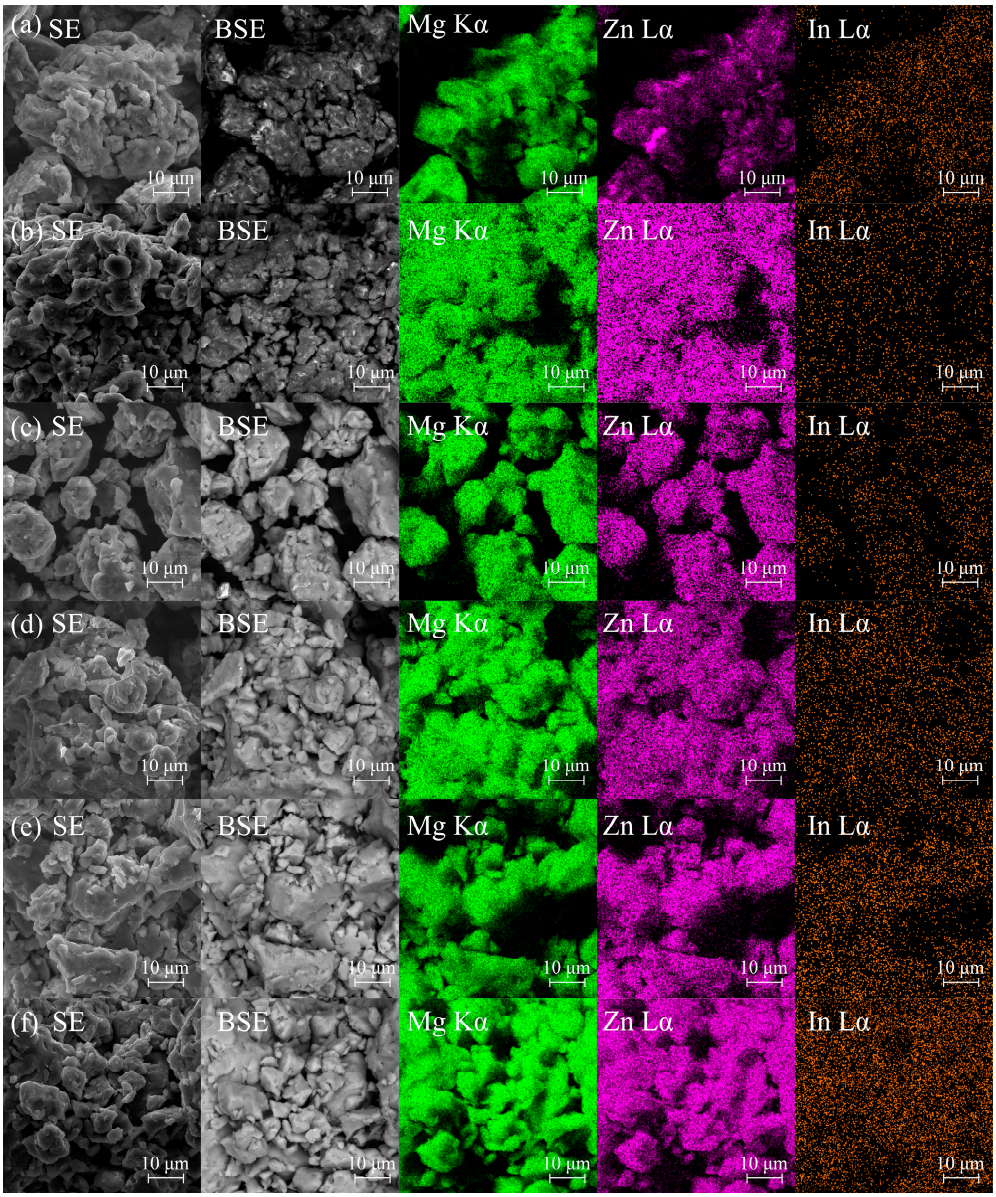

Figure 4. SEM images in secondary (SE) and backscattered (BSE) contrast combined with element distributions maps of the as-milled powders after different stages of mechanical alloying: 3 h (**a**), 6 h (**b**), 12 h (**c**), 24 h (**d**), 36 h (**e**), and 48 h (**f**).

Figure 5 displays the transformation of the crystallographic structure of the sintered alloys. The X-ray diffraction (XRD) patterns of the bulk Mg20Zn and Mg20Zn1In alloys are presented after being sintered at a temperature of 300 °C for 1 h. X-ray diffraction analysis of all the sintered materials consistently reveals the presence of a hexagonal close-packed magnesium-type structure with the following cell parameters: a = 0.320563 nm and c = 0.520527 nm (ICDD card no. 01-089-5003) and the $Mg_{51}Zn_{20}$ phase (ICDD card no. 00-007-1759). As the duration of milling increases, the dimensions of the unit cell gradually decrease and move towards smaller values. The unit cell parameters decrease to a = 0.320045 nm and c = 0.519716 nm for the alloy milled for 48 h, which can be attributed to the introduction of more defects into the structure with the prolonged mechanical alloying time (Table 2, Figure 5b,e). These alloys consist of $Mg_{51}Zn_{20}$ as a second phase. After the sintering process, it is possible to observe the unaltered alloy peak (101) that originates from the zinc.

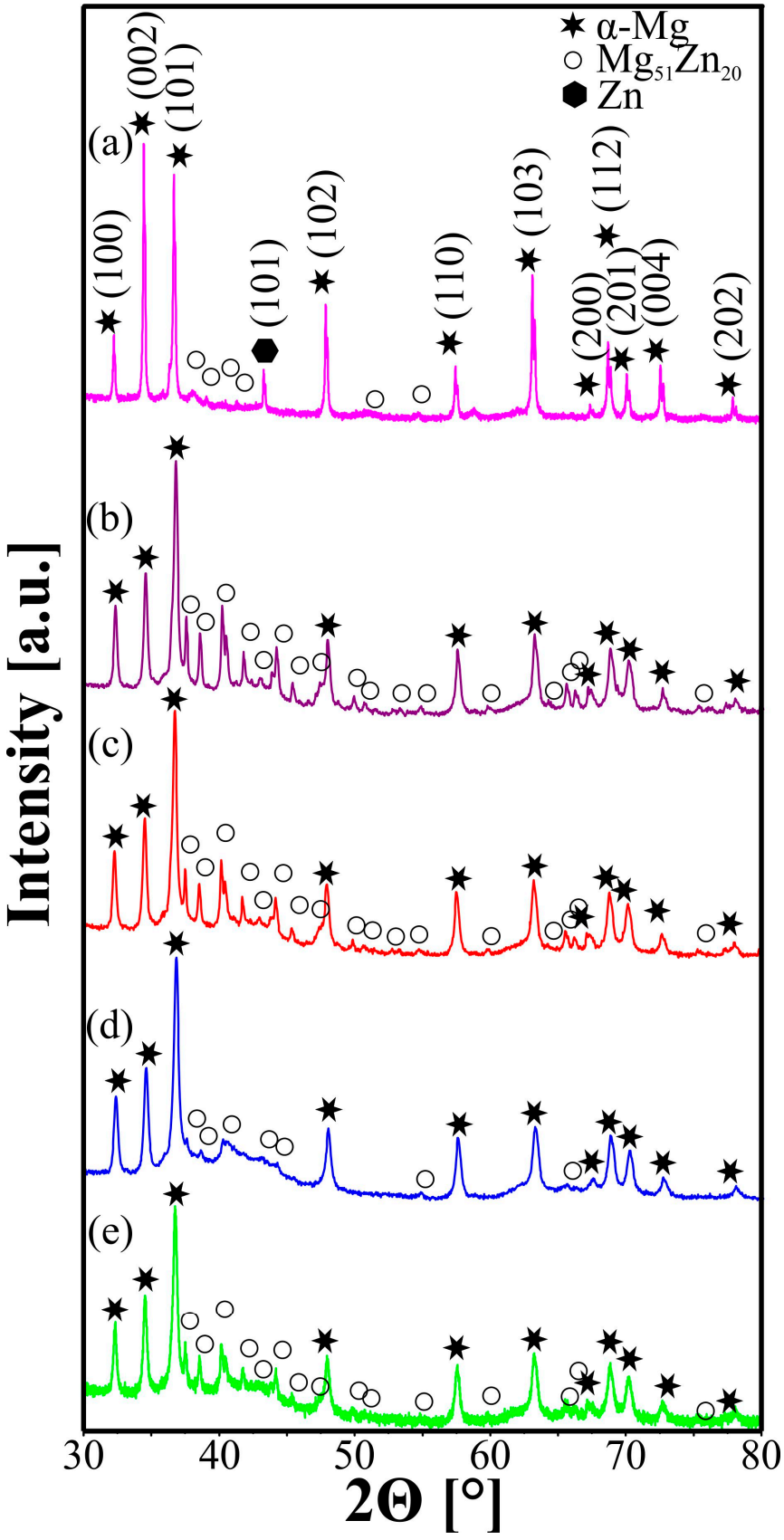

Figure 5. XRD patterns of the sinters: Mg-20Zn (**a**), Mg-20Zn-1In after 12 h (**b**), 24 h (**c**), 36 h (**d**), and 48 h (**e**) of MA.

Table 2. The unit cell dimensions, microhardness, theoretical, measured density, and porosity of the studied materials.

Sample	Mg-20Zn	Mg-20Zn-1In			
MA time [h]	48	12	24	36	48
a [nm]	3.20788	3.20563	3.20306	3.20341	3.20045
c [nm]	5.20883	5.20527	5.20099	5.20302	5.19716
$HV_{0.3}$	52 ± 3	134 ± 7	140 ± 7	143 ± 3	145 ± 3
ρ_{th} [g/cm^3]	2.047	2.0653			
ρ [g/cm^3]	1.99 ± 0.03	1.99 ± 0.02	1.99 ± 0.06	1.92 ± 0.02	1.96 ± 0.01
Porosity [%]	2.55 ± 0.02	3.43 ± 0.02	5.84 ± 0.02	7.02 ± 0.03	5.10 ± 0.04

Figure 6 shows the morphology of the sintered unmodified Mg-20Zn alloy. Except for the evenly distributed secondary $Mg_{51}Zn_{20}$ phase in the α-Mg matrix, small open microporosities are visible.

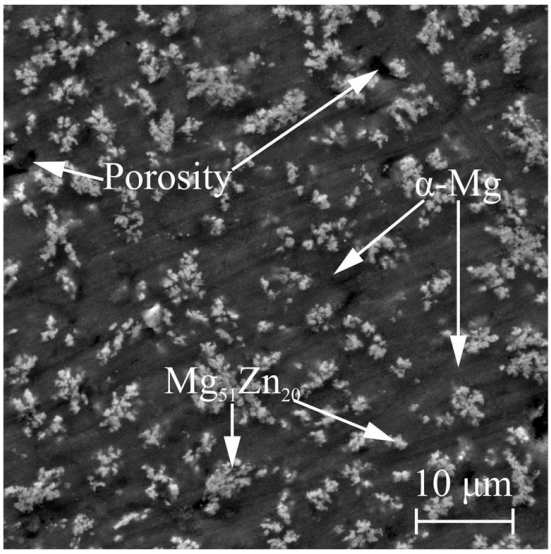

Figure 6. SEM image of the sintered Mg-20Zn.

Figure 7 depicts the morphology of the sintered alloys. All samples can be characterized by the even distribution of the $Mg_{51}Zn_{20}$ phase in the α-Mg matrix. For all of the samples, there are visible open porosities. The presence of porosities in the materials corresponds with the results of the density measurement. In general, the addition of indium with the prolonged time of milling led to an increase in porosity up to more than 7% for the sample milled for 36 h (Table 2).

The distribution of elements for the sintered alloy after 36 h is presented in Figure 8. All elements are homogeneously distributed in the materials. The EDS measurement confirms the presence of Zn and In in the α-Mg solid solution. Zinc is also concentrated in the $Mg_{51}Zn_{20}$ phase. The results revealed the presence of oxygen in the material, which can be related to the partial oxidation of materials during the mechanical alloying, sintering, and preparation of material for tests.

The results of the Vickers hardness test are shown in Table 2. The results show a significant increase in hardness after the addition of indium. They also show that an increase in the milling time can slightly improve the hardness of the materials. The sample after 12 h of MA has a hardness of 134 $HV_{0.3}$, while the sample after 48 h of MA has a higher value of 145.4 $HV_{0.3}$. The increase in hardness is caused by the change in crystalline size, a decrease in grain size to an ultrafine-grained structure, and changes in the microstructure. The presence of the $Mg_{51}Zn_{20}$ phase after sintering led to a significant increase in thw hardness values for all the indium-modified samples. The measured values are almost three times higher than those for the unmodified Mg-20Zn alloy (52 $HV_{0.3}$).

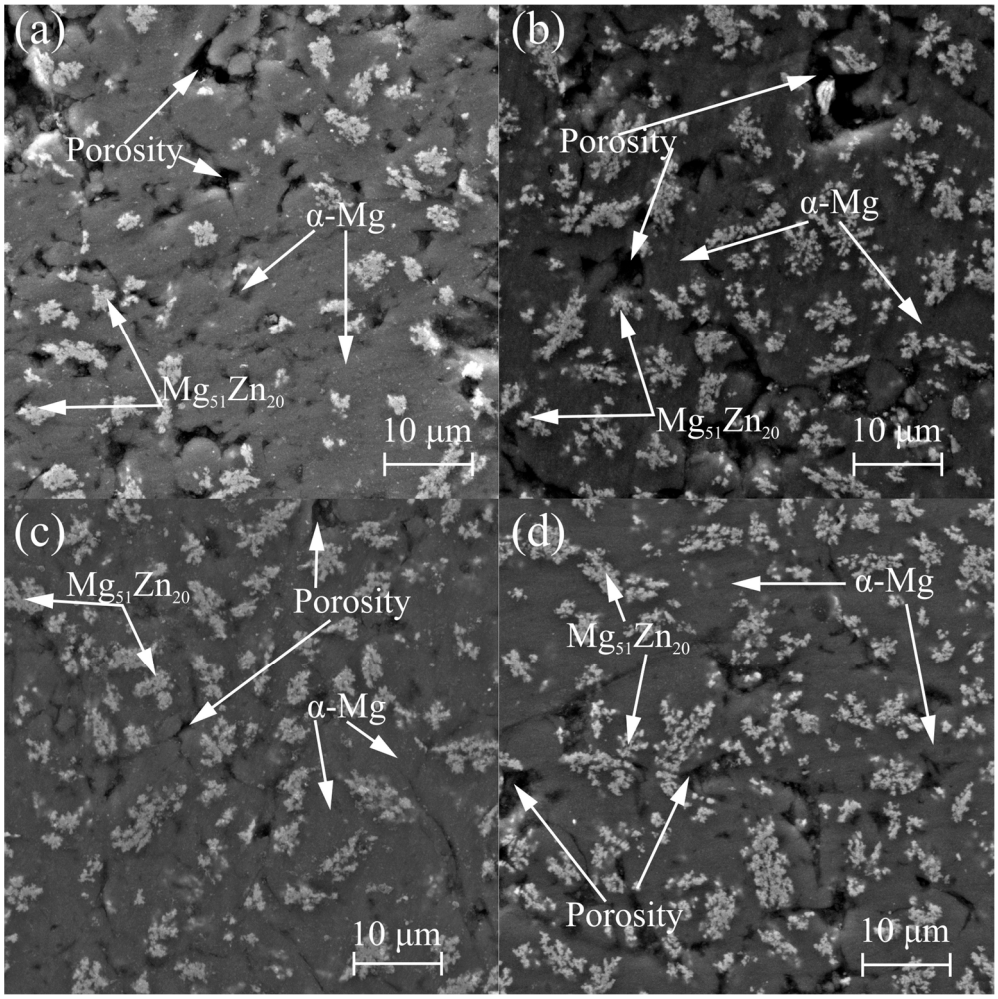

Figure 7. SEM images of the sintered Mg-20Zn-1In alloys after mechanical alloying: 12 h (**a**), 24 h (**b**), 36 h (**c**), and 48 h (**d**).

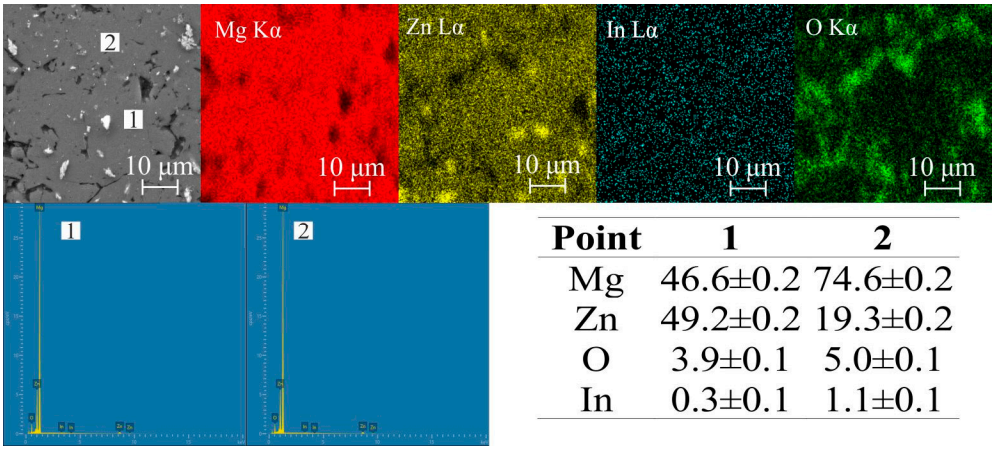

Point	1	2
Mg	46.6±0.2	74.6±0.2
Zn	49.2±0.2	19.3±0.2
O	3.9±0.1	5.0±0.1
In	0.3±0.1	1.1±0.1

Figure 8. EDS results of the Mg-20Zn-1n alloy after 36 h of MA.

All samples showed porosity after sintering—the maximum value calculated reached over 7% for the sample sintered after 36 h of the MA process. In general, with a prolonged mechanical alloying time, the porosity level is increased. In all samples with In, the porosity is higher than for the unmodified Mg-20Zn alloy (2.55% for the Mg-20Zn alloy and up to over 7% for the sample mechanically alloyed for 36 h).

The corrosion behavior in Ringer's solution at 37 °C was analyzed through the examination of polarization curves, which are depicted in Figure 9. The results of the potentiodynamic test are presented in Table 3. The unmodified Mg-20Zn alloy exhibits lower corrosion resistance than alloys containing indium (I_c = 2.937·10^{-4} [A/cm^2] and E_c = −1.740 [V]). The multiphase structure is responsible for the formation of galvanic coupling, which reduces the corrosion resistance of the materials. For alloys modified with indium, the corrosion potential is shifted to a less negative value (from −1.379 [V] for the alloy after 12 h of MA to −1.326 [V] for the alloy milled for 36 h.) The best corrosion properties are exhibited by the alloy after 36 h of MA I_c = 1.336·10^{-4} [A/cm^2], E_c = −1.326 [V].

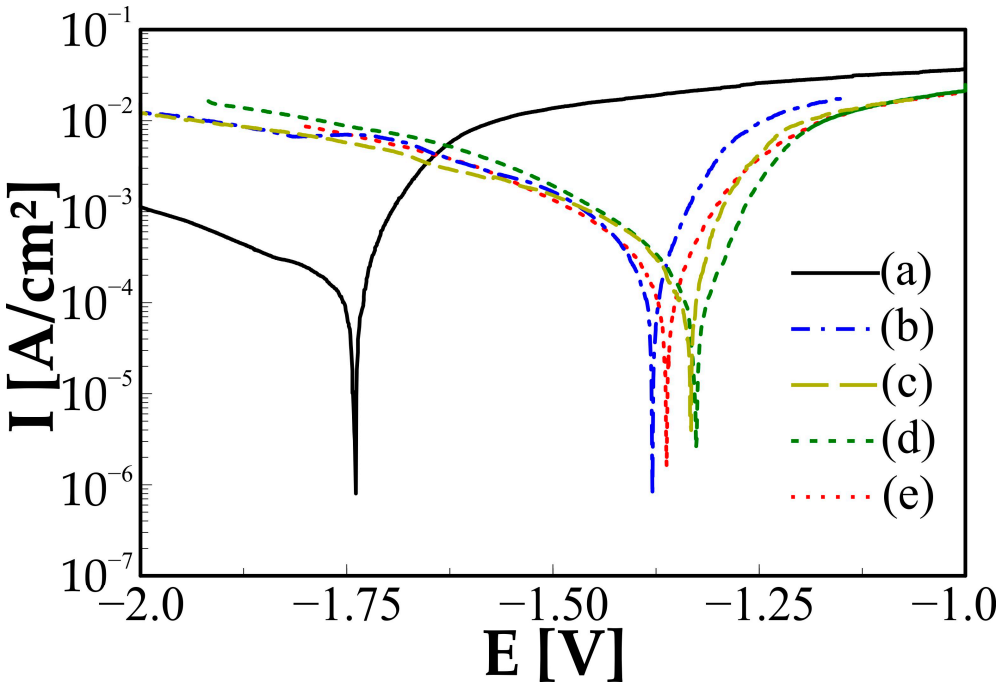

Figure 9. The potentiodynamic polarization curves of Mg-20Zn (a), Mg-20Zn-1In after 12 h (b), 24 h (c), 36 h (d), and 48 h (e) of MA.

Table 3. The values for the corrosion potential (E_c) and corrosion current density (I_c) of the synthesized alloys.

Sample	I_c [μA/cm^2]	E_c [V]
Mg-20Zn	293.7 ± 1.3	−1.74 ± 0.05
Mg-20Zn-1In -12 h MA	211.6 ± 3.2	−1.38 ± 0.04
Mg-20Zn-1In -24 h MA	178.9 ± 2.8	−1.33 ± 0.07
Mg-20Zn-1In -36 h MA	133.6 ± 7.4	−1.33 ± 0.03
Mg-20Zn-1In -48 h MA	176.4 ± 4.5	−1.36 ± 0.08

4. Discussion

There are various methods available for producing fine-grained structures, particularly in the production of magnesium alloys. A widely used strategy for achieving high-quality powders involves creating them at the nanometer scale, and they subsequently undergo consolidation through powder metallurgy methods. The processes of mechanical alloying, high-energy ball milling, and reactive milling can significantly reduce the size of microcrystalline materials, resulting in the production of nanocrystalline or ultrafine-grained structures.

Modifying the chemical composition of magnesium alloys is another commonly used approach to improving their mechanical and biological properties. The selection of appropriate alloying elements and the control of impurity levels are critical steps in enhancing the

corrosion resistance of magnesium alloys. Through these methods, magnesium alloys can be tailored to meet specific application requirements, such as in biomedical implants, where a combination of high strength, biocompatibility, and corrosion resistance is essential. As such, the research in this area continues to focus on developing new and improved methods for producing magnesium alloys with fine-grained structures and enhanced properties.

In this work, the mechanical alloying process, followed by pressing and sintering, was applied for the preparation of the bulk Mg20Zn and Mg20Zn1In alloys. The increase in hardness is caused by a decrease in grain size to ultrafine-grained structure and changes in the microstructure. The presence of the $Mg_{51}Zn_{20}$ phase after sintering led to a significant increase in hardness values for all indium-modified samples. Additionally, the unmodified Mg-20Zn alloy exhibits a lower corrosion resistance than alloys containing indium. The multiphase structure is responsible for the formation of galvanic coupling, which reduces the corrosion resistance of the materials. For alloys modified with indium, the corrosion potential is shifted to a less negative value, and the best corrosion properties are exhibited by the alloy after 36 h of MA ($I_c = 1.336 \cdot 10^{-4}$ [A/cm^2], $E_c = -1.326$ [V]).

The obtained results show the good prospective potential of Mg20Zn1In ternary alloys to be applied as biodegradable materials. The wettability and in vitro cytocompatibility will be investigated, and the results will be published independently.

5. Conclusions

The manufacturing process for the Mg-Zn-In alloy involves the implementation of mechanical alloying and the powder metallurgy procedure, which are both crucial for the production of high-quality materials. Through the process of MA, an intense level of deformation occurs, which ultimately results in the augmentation of the dislocation density. Additionally, this process leads to the formation of ultrafine grains. An improvement in properties caused by refining the structure and the addition of indium was observed. The current paper presents the effect of the addition of indium and mechanical alloying on the properties of the Mg-20Zn alloy. From the examination, the following conclusions can be drawn out:

(1) Indium enhances the properties of Mg-20Zn alloys—both the corrosion and the hardness;
(2) Samples with the addition of indium and milled for 36 h exhibit the best combination of properties;
(3) All samples containing indium offer a better corrosion resistance than the unmodified Mg-20Zn alloy.

Author Contributions: K.K., N.L., M.K. (Mateusz Kobus), M.K. (Mikolaj Kozlowski) and J.B. conducted the experimental and analytical works. K.K., N.L., M.K. (Mateusz Kobus), M.K. (Mikolaj Kozlowski) and M.J. wrote the manuscript. K.K. supervised the project. All authors have read and agreed to the published version of the manuscript.

Funding: The work was financed by the National Science Centre Poland under decision no. DEC-2017/27/N/ST8/01556.

Data Availability Statement: The data presented in this study are available on request from the corresponding author.

Conflicts of Interest: The authors declare no conflict of interest.

References

1. Sezer, N.; Evis, Z.; Kayhan, S.M.; Tahmasebifar, A.; Koç, M. Review of Magnesium-Based Biomaterials and Their Applications. *J. Magnes. Alloys* **2018**, *6*, 23–43. [CrossRef]
2. Amukarimi, S.; Mozafari, M. Biodegradable Magnesium-based Biomaterials: An Overview of Challenges and Opportunities. *MedComm* **2021**, *2*, 123–144. [CrossRef]
3. Mohamad Rodzi, S.N.H.; Zuhailawati, H.; Dhindaw, B.K. Mechanical and Degradation Behaviour of Biodegradable Magnesium–Zinc/Hydroxyapatite Composite with Different Powder Mixing Techniques. *J. Magnes. Alloys* **2019**, *7*, 566–576. [CrossRef]

4. Salama, M.; Vaz, M.F.; Colaço, R.; Santos, C.; Carmezim, M. Biodegradable Iron and Porous Iron: Mechanical Properties, Degradation Behaviour, Manufacturing Routes and Biomedical Applications. *J. Funct. Biomater.* **2022**, *13*, 72. [CrossRef]
5. Rabeeh, V.P.M.; Hanas, T. Progress in Manufacturing and Processing of Degradable Fe-Based Implants: A Review. *Prog. Biomater.* **2022**, *11*, 163–191. [CrossRef] [PubMed]
6. Hussain, M.; Ullah, S.; Raza, M.R.; Abbas, N.; Ali, A. Recent Developments in Zn-Based Biodegradable Materials for Biomedical Applications. *J. Funct. Biomater.* **2022**, *14*, 1. [CrossRef]
7. Nečas, D.; Marek, I.; Pinc, J.; Vojtěch, D.; Kubásek, J. Advanced Zinc–Magnesium Alloys Prepared by Mechanical Alloying and Spark Plasma Sintering. *Materials* **2022**, *15*, 5272. [CrossRef] [PubMed]
8. Zhang, T.; Wang, W.; Liu, J.; Wang, L.; Tang, Y.; Wang, K. A Review on Magnesium Alloys for Biomedical Applications. *Front. Bioeng. Biotechnol.* **2022**, *10*, 953344. [CrossRef]
9. Virtanen, S. Biodegradable Mg and Mg Alloys: Corrosion and Biocompatibility. *Mater. Sci. Eng. B* **2011**, *176*, 1600–1608. [CrossRef]
10. Wu, T.; Zhang, K. Corrosion and Protection of Magnesium Alloys: Recent Advances and Future Perspectives. *Coatings* **2023**, *13*, 1533. [CrossRef]
11. Brar, H.S.; Platt, M.O.; Sarntinoranont, M.; Martin, P.I.; Manuel, M.V. Magnesium as a Biodegradable and Bioabsorbable Material for Medical Implants. *JOM* **2009**, *61*, 31–34. [CrossRef]
12. Salleh, E.M.; Hussain, Z. *Effect of Zn Content on Biodegradable Mg Alloy Synthesized via Mechanical Alloying for Biomedical Application*; Springer: Berlin/Heidelberg, Germany, 2023; ISBN 9789811995088.
13. Yuan, W.; Xia, D.; Wu, S.; Zheng, Y.; Guan, Z.; Rau, J.V. A Review on Current Research Status of the Surface Modification of Zn-Based Biodegradable Metals. *Bioact. Mater.* **2022**, *7*, 192–216. [CrossRef] [PubMed]
14. Sotoudeh Bagha, P.; Khaleghpanah, S.; Sheibani, S.; Khakbiz, M.; Zakeri, A. Characterization of Nanostructured Biodegradable Zn-Mn Alloy Synthesized by Mechanical Alloying. *J. Alloys Compd.* **2018**, *735*, 1319–1327. [CrossRef]
15. Hernández-Escobar, D.; Champagne, S.; Yilmazer, H.; Dikici, B.; Boehlert, C.J.; Hermawan, H. Current Status and Perspectives of Zinc-Based Absorbable Alloys for Biomedical Applications. *Acta Biomater.* **2019**, 97. [CrossRef] [PubMed]
16. Mostaed, E.; Sikora-Jasinska, M.; Mostaed, A.; Loffredo, S.; Demir, A.G.; Previtali, B.; Mantovani, D.; Beanland, R.; Vedani, M. Novel Zn-Based Alloys for Biodegradable Stent Applications: Design, Development and in Vitro Degradation. *J. Mech. Behav. Biomed. Mater.* **2016**, *60*, 581–602. [CrossRef]
17. Yandong, Y.; Shuzhen, K.; Teng, P.; Jie, L.; Caixia, L. Effects of Mn Addition on the Microstructure and Mechanical Properties of As-Cast and Heat-Treated Mg-Zn-Ca Bio-Magnesium Alloy. *Metallogr. Microstruct. Anal.* **2015**, *4*, 381–391. [CrossRef]
18. Guleryuz, L.F.; Ipek, R.; Aritman, I. Effect of Ca Additions on the Mechanical Properties of Mg and in Vitro Degradation Behavior of Mg-XCa Alloys Produced by Powder Metallurgy. In Proceedings of the World PM 2016 Congress and Exhibition, Hamburg, Germany, 9–13 October 2016.
19. Salahshoor, M.; Guo, Y. Biodegradable Orthopedic Magnesium-Calcium (MgCa) Alloys, Processing, and Corrosion Performance. *Materials* **2012**, *5*, 135–155. [CrossRef] [PubMed]
20. Verissimo, N.C.; Brito, C.; Afonso, C.R.; Spinelli, J.E.; Cheung, N.; Garcia, A. Microstructure Characterization of a Directionally Solidified Mg-12wt.%Zn Alloy: Equiaxed Dendrites, Eutectic Mixture and Type/Morphology of Intermetallics. *Mater. Chem. Phys.* **2018**, *204*, 105–131. [CrossRef]
21. Jiang, P.; Blawert, C.; Zheludkevich, M.L. The Corrosion Performance and Mechanical Properties of Mg-Zn Based Alloys—A Review. *Corros. Mater. Degrad.* **2020**, *1*, 92–158. [CrossRef]
22. Becerra, A.; Pekguleryuz, M. Effects of Zinc, Lithium, and Indium on the Grain Size of Magnesium. *J. Mater. Res.* **2009**, *24*, 1722–1729. [CrossRef]
23. Zengin, H.; Turen, Y.; Ahlatci, H.; Sun, Y. Effect of Indium Addition on Microstructure and Mechanical Properties of AS-CAST and Hot-Rolled AM60 Magnesium Alloy. In Proceedings of the METAL 2017-26th International Conference on Metallurgy and Materials, Conference Proceedings, Brno, Czech Republic, 24–26 May 2017.
24. Wang, X.W.; Wang, W.; Chen, W.; Chen, D.M. Effects of Indium on Corrosion Behavior of Mg-Al-Cu Alloy. *Mater. Charact.* **2021**, *177*, 111157. [CrossRef]
25. Bao, T.; Hou, L.; Sun, J.; Liu, X.; Du, H.; Wei, H.; Wei, Y. Effect of Indium on the Negative Difference Effect for Magnesium Alloy. *J. Electrochem. Soc.* **2021**, *168*, 031515. [CrossRef]
26. Suryanarayana, C. Mechanical Alloying: A Critical Review. *Mater. Res. Lett.* **2022**, *10*, 619–647. [CrossRef]
27. Raducanu, D.; Cojocaru, V.D.; Nocivin, A.; Hendea, R.E.; Ivanescu, S.; Stanciu, D.; Trisca-Rusu, C.; Serban, N.; Drob, S.I.; Campian, R.S. Microstructure Evolution during Mechanical Alloying of a Biodegradable Magnesium Alloy. *Crystals* **2022**, *12*, 1641. [CrossRef]
28. Gonzaga, S.R.; Sedano, A.; Colín, J.M.; Torres-Islas, A.; Molina-Ocampo, A. Production of Biodegradable Mg-Based Alloys by Mechanical Alloying. *Dig. J. Nanomater. Biostruct.* **2021**, *16*, 1537–1545. [CrossRef]
29. Lesz, S.; Karolus, M.; Gabryś, A.; Kremzer, M. Influence of Milling Time on Phase Composition and Product Structure of Mg-Zn-Ca-Ag Alloys Obtained by Mechanical Synthesis. *Materials* **2022**, *15*, 7333. [CrossRef]
30. Lesz, S.; Karolus, M.; Gabryś, A.; Hrapkowicz, B.; Walke, W.; Pakieła, W.; Gołombek, K.; Popis, J.; Palček, P. Characteristics of Mg-Based Sintered Alloy with Au Addition. *Materials* **2023**, *16*, 1915. [CrossRef]
31. Salleh, E.M.; Ramakrishnan, S.; Hussain, Z. Synthesis of Biodegradable Mg-Zn Alloy by Mechanical Alloying: Effect of Milling Time. *Procedia Chem.* **2016**, *19*, 525–530. [CrossRef]

32. Yang, Y.; Wang, W.; Yang, M.; Yang, Y.; Wang, D.; Liu, Z.; Shuai, C. Laser-Sintered Mg-Zn Supersaturated Solid Solution with High Corrosion Resistance. *Micromachines* **2021**, *12*, 1368. [CrossRef]
33. Hu, Y.; Guo, X.; Qiao, Y.; Wang, X.; Lin, Q. Preparation of Medical Mg–Zn Alloys and the Effect of Different Zinc Contents on the Alloy. *J. Mater. Sci. Mater Med.* **2022**, *33*, 9. [CrossRef]
34. Youssef, K.M.; Wang, Y.B.; Liao, X.Z.; Mathaudhu, S.N.; Kecskés, L.J.; Zhu, Y.T.; Koch, C.C. High Hardness in a Nanocrystalline Mg97Y2Zn1 Alloy. *Mater. Sci. Eng. A* **2011**, *528*, 7494–7499. [CrossRef]
35. Hwang, S.; Nishimura, C.; McCormick, P.G. Mechanical Milling of Magnesium Powder. *Mater. Sci. Eng. A* **2001**, *318*, 22–33. [CrossRef]
36. Kowalski, K. Effects of Mechanical Alloying Conditions on the Properties of Mg-Based Nanomaterials. *Inżynieria Mater.* **2015**, *1*, 23–26. [CrossRef]
37. Kowalski, K.; Nowak, M.; Jakubowicz, J.; Jurczyk, M. The Effects of Hydroxyapatite Addition on the Properties of the Mechanically Alloyed and Sintered Mg-RE-Zr Alloy. *J. Mater. Eng. Perform.* **2016**, *25*, 4469–4477. [CrossRef]
38. *PN-EN ISO 6507-1:2018-05*; Metallic materials- Vickers hardness test- Part 1: Test method. PKN: Warsaw, Poland, 2018.